



Low-power swept-source Raman spectroscopy

AMIR H. ATABAKI,^{1,*} WILLIAM F. HERRINGTON,¹ CHRISTOPHER BURGNER,² VIJAYSEKHAR JAYARAMAN,² AND RAJEEV J. RAM¹

¹*Massachusetts Institute of Technology, Cambridge, MA 02139, USA*

²*Praevium Research, Inc. Goleta, CA 93117, USA*

*atabaki@mit.edu

Abstract: ‘Molecular fingerprinting’ with Raman spectroscopy can address important problems—from ensuring our food safety, detecting dangerous substances, to supporting disease diagnosis and management. However, the broad adoption of Raman spectroscopy demands low-cost, portable instruments that are sensitive and use lasers that are safe for human eye and skin. This is currently not possible with existing Raman spectroscopy approaches. Portability has been achieved with dispersive Raman spectrometers, however, fundamental entropic limits to light collection both limits sensitivity and demands high-power lasers and cooled expensive detectors. Here, we demonstrate a swept-source Raman spectrometer that improves light collection efficiency by up to 1000× compared to portable dispersive spectrometers. We demonstrate high detection sensitivity with only 1.5 mW average excitation power and an uncooled amplified silicon photodiode. The low optical power requirement allowed us to utilize miniature chip-scale MEMS-tunable lasers with close to eye-safe optical powers for excitation. We characterize the dynamic range and spectral characteristics of this Raman spectrometer in detail, and use it for fingerprinting of different molecular species consumed everyday including analgesic tablets, nutrients in vegetables, and contaminated alcohol. By moving the complexity of Raman spectroscopy from bulky spectrometers to chip-scale light sources, and by replacing expensive cooled detectors with low-cost uncooled alternatives, this swept-source Raman spectroscopy technique could make molecular fingerprinting more accessible.

© 2021 Optical Society of America under the terms of the [OSA Open Access Publishing Agreement](#)

1. Introduction

Raman spectroscopy has been a trusted tool for realtime molecular analysis in many industries for decades—from forensics and security [1] to pharmaceutical and semiconductor [2]. More recently, Raman spectroscopy has been shown to be a powerful tool for addressing some of the pressing challenges in agriculture, healthcare, and therapeutics: it can enable precision agriculture [3], label-free and in vivo cancer screening [4], and new paradigms in pharmaceutical manufacturing [5]. This approach can also help identify food and drug contamination that cause human loss around the world [6]. But to have any practical impact, Raman spectroscopy should become widely accessible, and therefore, needs to be low-cost, compact, low-power (both electrical and optical) while retaining its performance. Today’s Raman instruments cannot offer these capabilities simultaneously.

The challenge of building an accessible sensitive Raman instrument—i.e., low-cost, compact, low-power, sensitive—starts from the inefficiency of the Raman scattering process—one out of a million to a billion incident photons undergoes Raman scattering. This problem is exacerbated by the diffuse scattering of Raman photons in most inhomogeneous samples, requiring large spectroscopic instruments to achieve high collection efficiency for photons that are spread over a large area and solid angle. The Constant Radiance Theorem dictates this latter entropic limit to light collection efficiency [7]. Together, the low Raman signal and collection efficiency limit, necessitate the use of either powerful excitation lasers, large high-throughput spectrometers, or low-noise cooled detectors to achieve adequate signal to noise ratio and sensitivity. In practice,

most systems combine at least two of these elements to achieve an acceptable performance. These lasers exceed eye exposure limits by about 100×, spectrometers are subject to size-throughput trade-offs, and the cooled detectors are power-inefficient and expensive. This has led to Raman spectrometers that are large, expensive and use lasers that cannot be operated without precaution.

Surface enhanced Raman spectroscopy (SERS) [8] and Fourier Transform Raman (FT-Raman) spectroscopy [9,10] have been pursued to address the limitations imposed by weak Raman signals. SERS enhances the Raman signal by as much as 10^{14} and allows Raman sensing with single molecule sensitivity. However, SERS is no longer reagentless, contactless, or general, as it typically requires chemical binding of the analyte to the metallic nanostructure, and therefore, inapplicable to solid samples. FT-Raman preserves the benefits of traditional dispersive spectroscopy of spontaneous Raman scattering—reagentless, contactless, and general—while still improving sensitivity due to both a high light-collection capability (throughput gain), and detection of the whole spectrum at once (multiplexing gain) [9]. However, the moving mirror in FT-Raman makes it less robust compared to dispersive Raman spectrometers that have dominated the field in recent years.

In nonlinear Raman spectroscopy, such as coherent anti-stokes Raman spectroscopy (CARS) and stimulated Raman spectroscopy (SRS), tunable lasers have been used to eliminate the spectrometer [11,12] and address its throughput limitations. However, the high-peak powers needed in nonlinear spectroscopies have necessitated high-power benchtop optically-pumped lasers and light sources [11,12]. Even systems using portable supercontinuum fiber sources and ultrafast pulse-shapers cannot be handheld because of size and power consumption.

In this work, we demonstrate that the use of tunable sources and elimination of the spectrometer can be brought from nonlinear spectroscopies to spontaneous Raman spectroscopy and enable compact, sensitive, and low-power instruments. The enabling part of this swept-source approach is a high optical throughput design that lowers laser excitation requirement to milliwatt range, allowing us to utilize chip-scale tunable lasers. The high optical throughput also allows us to use uncooled photodiodes instead of cooled charged coupled devices (CCDs) and still achieve high detection sensitivity. This is a major step towards reducing the cost of Raman spectrometers. Together, the compact and low-power laser and detector used in this work show the potential of Swept-source Raman Spectroscopy (SSRS) for bringing Raman spectroscopy out of laboratories and making it more accessible.

2. Concept and optical throughput analysis

The SSRS concept shown in this work uses a tunable laser source for excitation and narrowband detection—the reverse of dispersive and FT Raman spectrometers in which a fixed-wavelength laser and broadband detection is used. Here, we use a dispersive Raman spectrometer to demonstrate the SSRS concept. Figure 1 shows the Raman spectrum of acetaminophen as the excitation wavelength is increased from right to left. By placing a narrow bandpass filter in the system (marked by the cyan band) and sweeping the excitation wavelength, the entire Raman spectrum of acetaminophen can be swept across this one spectral band. We added this filter to our setup and integrated the Raman photons on the spectrometer. The Raman spectrum acquired with this swept-source concept is shown in the inset (blue) and compared with that of a dispersive Raman spectrometer (red). The two spectra are consistent and the slight amplitude differences are due to filter response differences for these two experiments.

The advantage of the SSRS approach is that it can enable strong collection efficiency beyond dispersive and FT spectrometers. The reason is that the spectral filtering in SSRS can be achieved with Fabry-Perot (FP) interference filters with a spectral response that is less sensitive to the incidence angle compared to diffraction gratings (in dispersive spectrometers) or Michelson interferometers (in FT spectrometers). The throughput advantage of FT spectrometers over dispersive spectrometers has been known for a while [10].

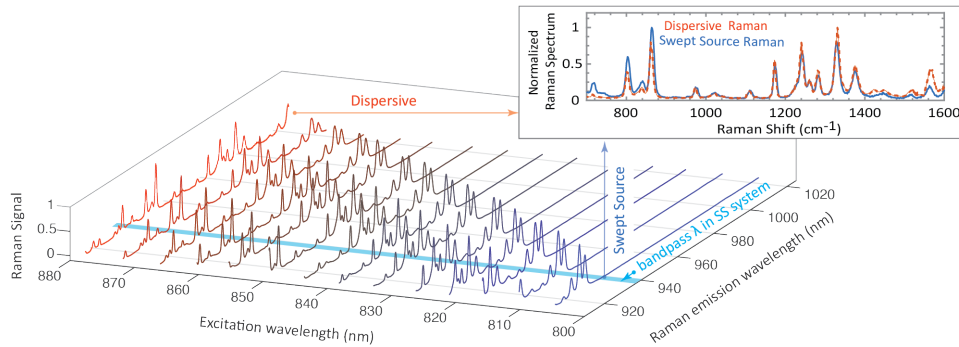


Fig. 1. Swept source Raman spectroscopy concept. Raman spectra of acetaminophen acquired with a conventional benchtop dispersive spectrometer and high-power tunable laser. As the excitation wavelength is swept from right to left, the Raman peaks of acetaminophen are swept across the position of the cyan band. The cyan band marks the position of the narrowband filter that selects the only spectral channel in SSRS. This filter is placed in the setup and the Raman spectra of acetaminophen are acquired as the laser is swept. The spectrum that is acquired through this swept-source approach is shown in inset (blue) and compared with the spectrum from the dispersive approach (red).

In [Supplement 1](#) we provide a detailed theory for the throughput comparison of SSRS with FT spectrometers. This theory shows that the spectral resolution of both of these systems is $\Delta\lambda_{\text{FWHM}} = \lambda_0 [a/(2fn^*)]^2$, where a is the size of the input aperture, f is the focal length of the first collimating lens, and n^* is the effective index that the beam sees in the filtering element of each spectrometer—i.e., free-space Michelson interferometer in FT and FP interference filter in SSRS. $n^* = 1$ for FT spectrometer and $n^* = 1.58$ for the FP interference filter used in our SSRS setup. The higher refractive index of the interference filter reduces the sensitivity to incidence angle and allows a larger input aperture for the same spectral resolution. We also show in [Supplement 1](#) that the etendue (throughput) of both of these systems can be calculated by $S = [\pi(\text{NA})fn^*]^2 R^{-1}$, where NA is the numerical aperture of the input lens, and $n^* = 1$ for FT spectrometer and $n^* = 1.58$. This theory explains the throughput advantage of SSRS (at a single spectral channel) over a FT spectrometer.

Figure 2 compares the theoretical optical throughput (etendue) of SSRS with dispersive, and FT Raman at a single spectral channel. We assumed a wide range of parameters used in three different classes of dispersive spectrometers—compact-handheld, portable, benchtop. For a fair comparison of FT-Raman and SSRS we assumed the same numerical aperture for the collection and detection lenses in these systems [see Fig. 2(a) for the schematic and refer to [Supplement 1](#) for the details of throughput calculation and the comparison].

The optical throughput of SSRS can be 20× and 1000× higher than benchtop and compact handheld dispersive Raman spectrometers, respectively. SSRS can also offer higher throughput than FT at any spectral resolution above 6 cm^{-1} . This narrowband throughput gain leads to a sensitivity advantage in many applications where only a small set of Raman bands are monitored and contain information [11,12]. Also, for broadband applications the total acquisition time would be comparable with dispersive Raman spectrometers despite needing wavelength sweeping. This is because with 20× throughput advantage versus benchtop spectrometers, the integration time per spectral point for SSRS can be as short as 1/400 of the total acquisition time of the dispersive system to achieve the same SNR—noise scales with the square root of integration time. Therefore, a few hundred wavelength points can be scanned with SSRS during the acquisition time of the dispersive system, leading to a similar spectral acquisition time for both systems.

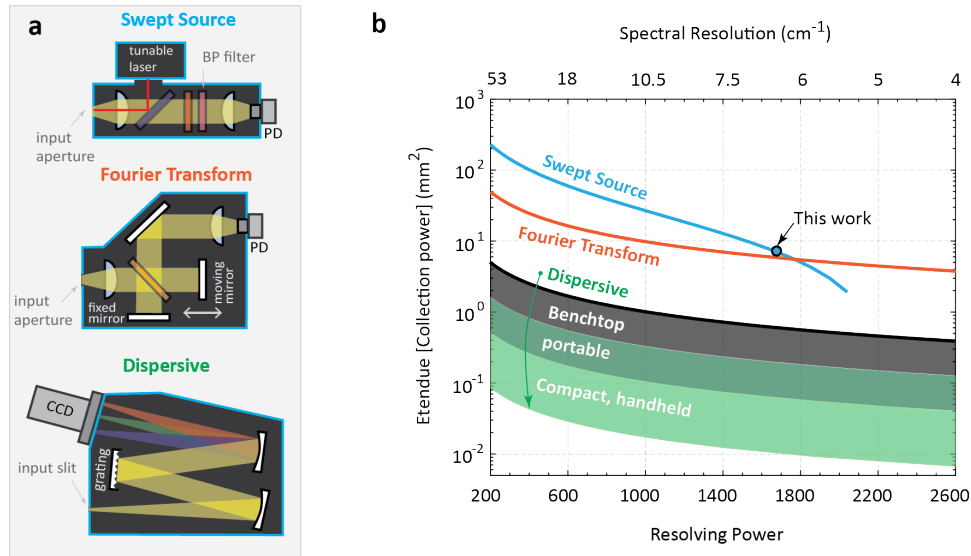


Fig. 2. Comparison of the throughput of Raman spectroscopy systems at one spectral channel (a) Schematic of three spontaneous Raman spectroscopy systems. (b) Comparison of the etendue (light collection power) of spectroscopy systems shown in (a) at a single spectral channel versus resolving power. The analysis of SSRS is based on the properties of optical components in our experimental setup shown in Fig. 3(a). For FT spectrometer we assumed similar optical components as those used in the analysis of the swept source approach. For dispersive spectrometers, a wide range of parameters for benchtop, portable, and compact-handheld instruments are used. See [Supplement 1](#) for details of analysis. The top x axis shows the spectral resolution.

Nevertheless, SSRS still preserves its sensitivity advantage for most narrowband applications [11,12].

3. Design

Our goal is to leverage the throughput advantage of the SSRS architecture to design an instrument with high sensitivity, uncooled detectors, and low-power excitation (eye-safe-level). These criteria have not been achieved simultaneously in any instrument and are important for the broad adoption of Raman spectrometers outside of laboratory settings. Most Raman spectrometers (laboratory-scale or handheld) use hundreds of mW of optical power, which is more than 100 \times higher than the human eye exposure limit. Even with such high optical powers, cooled detectors are needed to compensate for the low throughput of dispersive spectrometers. The 1000 \times throughput advantage of the swept-source architecture compared to existing handheld systems [Fig. 2(b)] allows us to both reduce excitation power by 100 \times and use uncooled detectors without compromising sensitivity.

Figure 3(a) shows the three-dimensional schematic of the of our SSRS instrument [experimental setup shown in Figs. 3(e) and 3(f)]. The excitation source from the MEMS-tunable laser is delivered to our SSRS probe using an optical fiber. The MEMS-tunable laser is a vertical cavity surface emitting laser (VCSEL) with a cavity length of a few wavelengths and a device diameter of about 200 μm [Figs. 3(b) and 3(e)]. The Raman probe is used for excitation of the sample,

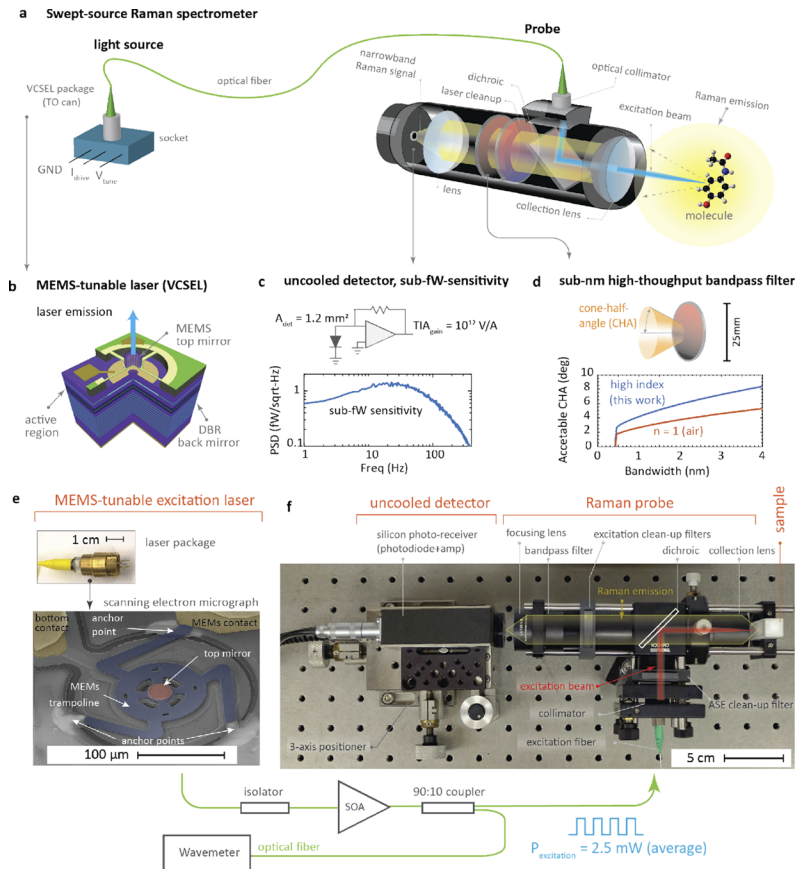


Fig. 3. (a) Schematic of the swept-source Raman spectrometer. The excitation source (left) is a chip-scale MEMS-tunable vertical cavity surface emitting laser (VCSEL)—schematic is shown in (b). The probe is used for excitation, collection and detection of the Raman emission. The Raman probe uses a single-element photodiode (c) in conjunction with a high-throughput thin-film interference filter (d) to collect and detect a single spectral channel with high optical throughput. (b) Layout of the MEMS-tunable VCSEL used in this work [13,14]. (c) The unbiased photodiode with a high transimpedance gain of 10^{12} V/A. Plot shows a sub-fW/ $\sqrt{\text{Hz}}$ power spectral density for the dark noise of the detector and amplifier. (d) The Interference bandpass filter used for SSRS has high light collection power because of its large area (25-mm-diameter) and a high acceptable cone-half-angle (CHA) of 3° for a target bandwidth of 0.5 nm. Blue curve shows the simulated acceptable CHA versus bandwidth for the filter used in this work. These interference filters have a higher acceptable CHA compared to Michelson interferometers used in FT and spatial heterodyne spectrometers [15] (red curve). (e) Photo and scanning electron micrograph of chip-scale MEMS-tunable laser used in our swept source setup. We used two such VCSELS to cover 400 cm^{-1} of spectral range in our experiments. The laser current is chopped with 50% duty-cycle for lock-in detection and the laser output is amplified to 3 mW with a semiconductor optical amplifier before entering the Raman spectroscopy setup in (a). A 90:10 coupler is used to monitor the wavelength of the tunable source with a wavemeter. (f) Experimental setup of the SSRS system. The optical assembly on the right is used for excitation, collection, and bandpass filtering of Raman emission. The silicon detector on the left is placed on a 3-axis positioner for alignment with the excitation spot on the sample (cuvette on the right). All filters and lenses have a diameter/width of 25 mm.

as well as, collection, filtering and detection of the Raman emission. We use a back-scattered geometry for excitation-collection where a dichroic filter is used to send the excitation light along the collection-detection axis. A narrowband bandpass interference filter is placed along the optical axis to select one Raman spectral channel prior to detection.

The narrowband filter that selects the Raman channel plays a critical part in the overall performance of the spectroscopy system. The spectral resolution of the system is inversely proportional to the bandwidth of this filter. At the same time, the bandwidth of the filter depends on the cone-angle of the incident light [Fig. 3(d)], which together with the area of the filter determine the throughput of the optical setup. The tradeoff seen between the spectral resolution and throughput for the swept-source architecture in Fig. 2(b) is due to this dependence of filter bandwidth on incident cone-angle. We use a narrowband Fabry-Perot (FP) interference filter (from Alluxa) that provide both high spectral resolution (5 cm^{-1}) and high overall throughput. See [Supplement 1](#) for our theoretical analysis of the throughput advantage of these filters.

The throughput advantage of SSRS allows us to tolerate more detector noise and use low-cost, uncooled detectors instead of photon counting devices such as cooled charge coupled devices (CCDs). Here, we use a single-element amplified uncooled photodiode with an area of 1.2 mm^2 . The detector area coupled with a high numerical aperture lens provides enough collection power to detect all of the photons within the acceptable cone-angle of the bandpass filter. However, even with such a high throughput architecture, the Raman signal is typically between 1 fW to 1 pW per mW of excitation power for a single Raman line. By using a very-high transimpedance gain of 10^{12} with a large-area zero-biased photodiode (Femto GmbH), sub-fW detection sensitivity can be achieved [Fig. 3(c)]. Such a high gain level reduces noise but limits the bandwidth to 20 Hz which is acceptable for most Raman spectroscopy experiments.

4. Experimental results

Figure 3(f) shows the experimental setup of the SSRS system with the MEMS-tunable laser [Fig. 3(e)]. The laser wavelength is tuned by electrostatically changing the cavity length through the top laser mirror, which is fabricated on a suspended MEMS structure [13,14]. See [Supplement 1](#) for the details of the laser structure. We used two MEMS-tunable lasers near 850 nm that together provided 400 cm^{-1} of Raman shift in our experiments. These MEMS-tunable lasers typically need amplification and have been co-packaged with optical amplifiers in a single compact package [16]. Our lasers did not have an integrated amplifier and therefore we used a discrete semiconductor optical amplifier to increase the excitation power to $3\text{-}5\text{ mW}$ throughout the tuning range of the lasers. Also, these lasers are not temperature stabilized; therefore, we used a wavelength meter to monitor their wavelength and to calibrate the Raman shift in our measurements in realtime (setup details in [Supplement 1](#)).

We used high numerical aperture lenses ($\text{NA} = 0.63$) with a diameter of 25 mm for the 2 lenses close to the sample and detector. With this numerical aperture and a detector area of about 1.2 mm^2 , the etendue (optical throughput) of the detector matches the etendue of the bandpass interference filter. Together, they ensure a high overall optical throughput for the system. We also used fixed short-pass and long-pass bandedge filters as amplified spontaneous emission (ASE) and excitation cleanup. This eliminated the need for tunable filters which were believed to be one of the challenges of using tunable sources in Raman spectroscopy [17]. We chopped the laser current at 10 Hz and performed lock-in detection, which both reduced detector noise by about $2\times$ and made the setup less sensitive to ambient light. While all of our experiments were conducted in a light-tight box for repeatability, we observed minor changes in the Raman signal when the setup was exposed to fluorescent room lights.

Figure 4(a) shows the Raman spectrum of acetaminophen acquired with our SSRS setup with an integration time of 0.1 s per spectral point (6 s acquisition time for the whole spectrum). We superimpose the Raman spectrum acquired with a benchtop dispersive spectrometer for

comparison (dotted red curve). The Raman peaks with the two instruments align with a high accuracy. Figures 4(b) and 4(c) show signal and spectral characteristics of the SSRS system measured using toluene. The laser wavelength was tuned such that the 1003 cm^{-1} Raman line of toluene overlaps with the bandpass filter. With only 3 mW of peak excitation power (average power of 1.5 mW with 50% duty cycle modulation), a 1.2-V_{pp} signal was measured at the output of the detector corresponding to 2 pW peak Raman signal [Fig. 4(b)]. We swept the laser across the 1003 cm^{-1} band and estimated a spectral resolution of 5 cm^{-1} for our SSRS setup after accounting for the intrinsic 1.9 cm^{-1} linewidth of this Raman line [Fig. 4(c)]. Figure 4(d) shows the power spectral density of the detector in dark and after receiving Raman light from the 1003 cm^{-1} band. A dynamic range of $23\text{ dB}/\sqrt{\text{Hz}}$ is observed, which corresponds to an SNR of 23 dB for an integration time of 0.5 s per spectral point. The Raman spectrum of toluene across the tuning range of the MEMS VCSELs is shown in Fig. 5(a) next to the spectra of other reference standards. The total spectral acquisition time is 6 s with an average excitation power of 1.5-2.5 mW.

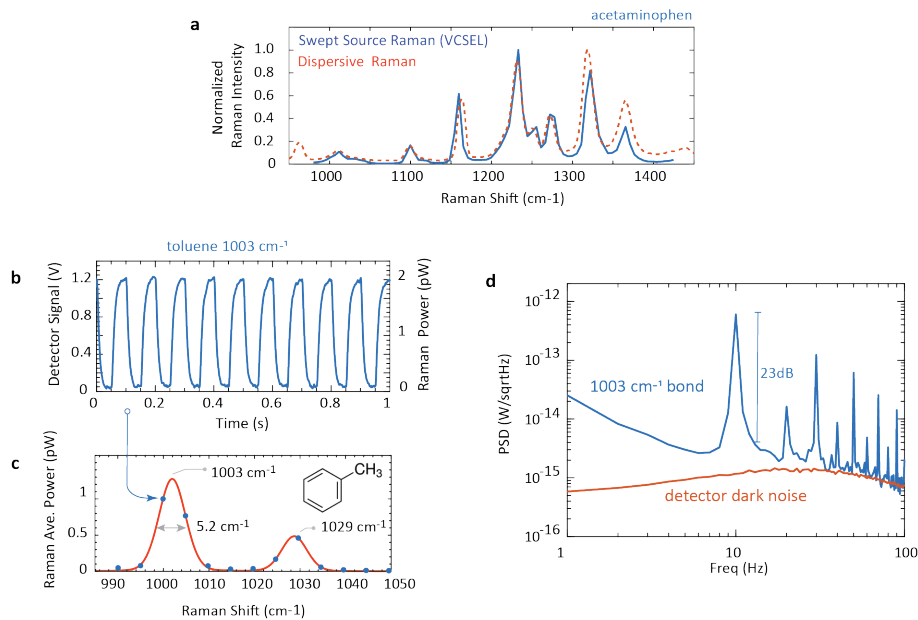


Fig. 4. (a) Raman spectrum of acetaminophen (blue curve) measured with the SSRS setup and amplified VCSEL lasers with a maximum average optical power of 2.5 mW (max peak power 5 mW). Dispersive Raman spectrum is also shown in dashed red curve for comparison. Slight differences in Raman peak heights is due to the optical filters that affect each acquisition differently. (b) Detector signal for toluene 1003 cm^{-1} Raman line. Peak voltage of 1.2 V corresponds to 2 pW peak received Raman power. (c) The VCSEL wavelength was swept with 0.36 nm resolution across two Raman lines of toluene with an average power of 1.5 mW (max peak power 3 mW). The measured FWHM of the 1003 cm^{-1} line is 5.2 cm^{-1} . The red curve is a mixed Gaussian-Lorentzian (Voigt) lineshape fitted to the experimental data (circles). (d) Power spectral density (PSD) of the Raman signal for the 1003 cm^{-1} line (blue) showing about $23\text{ dB}/\sqrt{\text{Hz}}$ of dynamic range with respect to the noise floor. PSD of the detector dark noise is shown in red.

The low power requirement of SSRS (for both the laser and detector) with a potentially compact formfactor using chip-scale MEMS-tunable lasers makes this approach appealing for consumer applications. Here, we consider three classes of molecules that are commonly ingested:

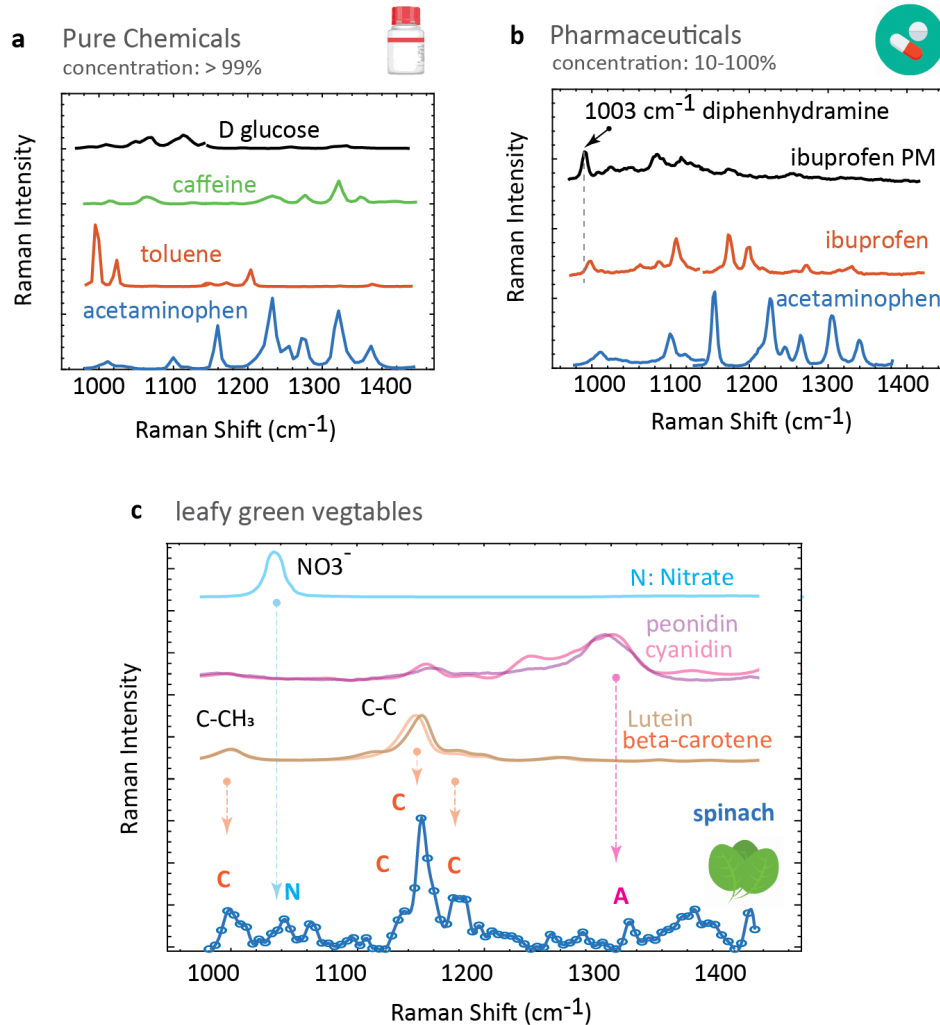


Fig. 5. SSRS results for molecular fingerprinting at different concentration levels. All spectra acquired with amplified VCSELs with a maximum average power of 2.5 mW (max peak power 5 mW). (a) Spectra of reference standards of four pure chemicals each acquired in a total of 6 s (0.1 s integration time per point). (b) Spectra of three different analgesics acquired in a total of 6 s (0.1 s integration time per point). (c) Raman spectrum from a spinach leaf (blue) with carotenoid (C), anthocyanin (A), and nitrate (N) peaks annotated. The spectrum is the average of two spectra each acquired in a total of 52 s (1 s integration time per point). The fluorescence background is approximated and subtracted using a fifth-order polynomial. The Raman spectra of some chemical components of spinach used for peak assignments are shown on top: carotenoids lutein and beta-carotene, anthocyanins peonidin and cyanidin, and nitrate.

analgesics [Fig. 5(b)], nutrients in vegetables [Fig. 5(c)], and alcoholic beverages [Fig. 6(a)]. The ability to verify and quantify these chemicals in our daily lives could save significant health consequences. The World Health Organization estimates that about 10% of medicine in low- and middle-income countries is substandard or falsified, and is the cause of death of hundreds of thousands of children annually [18]. Similarly, outbreaks of methanol poisoning in alcoholic beverages occur frequently around the world and disproportionately affect the poor in developing and developed countries [6]. On the other hand, several critical nutrients such as carotenoids in leafy-vegetables are anti-oxidants with numerous health benefits such as cancer resistance. We demonstrate that the SSRS instrument with a low-power, MEMS VCSEL can identify these important classes of molecules ingested commonly in our daily lives.

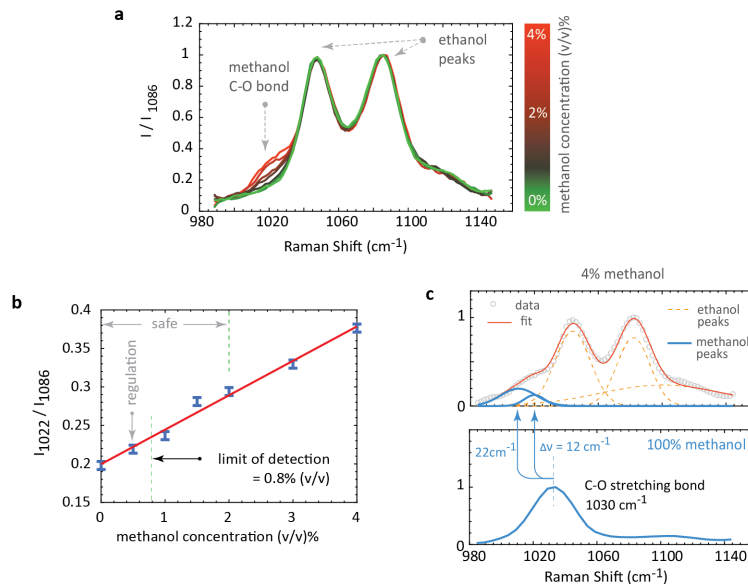


Fig. 6. Measurement of the LOD of methanol All spectra acquired with a single amplified VCSEL with a maximum average power of 1.5 mW (max peak power 3 mW) (a) Spectra of vodka (40% alcohol by volume) spiked with different concentrations of methanol from 0.5% to 4% (v/v) acquired in a total of 32 s each (1 s integration time per point). Methanol's C-O stretching bond creates a shoulder on the left side of two ethanol peaks. All spectra are normalized to the ethanol peak at 1086 cm^{-1} (b) Ratio of Raman intensity at 1020 cm^{-1} to 1086 cm^{-1} is used to estimate the LOD of methanol. These two spectral points are integrated for 5 s (total acquisition time of 10 s). An LOD of 0.8% (v/v) is achieved, which is below the safety consumption level of 2%. (c) Top: Raman spectrum of vodka containing 4% methanol. Spectrum is decomposed on a series of Gaussian peaks. Dotted orange and blue curves are contributions of ethanol and methanol peaks. Bottom: Raman spectrum of methanol. The C-O stretching bond of methanol at 1030 cm^{-1} is red-shifted by 12 cm^{-1} and 22 cm^{-1} to 2 new peaks when mixed with vodka.

We acquired Raman spectra of over-the-counter analgesics with 0.1 s integration time per spectral point [6 s for the whole spectrum, Fig. 5(b)]. We could distinguish two similar pharmaceutical tablets (ibuprophen and ibuprophen PM) from the antihistamine (diphenhadramine) peak near 1003 cm^{-1} that is present in only one of these tablets (ibuprophen PM). Previous demonstrations of the analysis of pharmaceuticals with dispersive Raman spectrometers by various food, drug and health organizations worldwide have required cooled detectors (-40°) and approximately 100 \times more excitation power than our work (for a comparable integration time) [19–21].

We then analyzed leafy vegetables with many molecular species that impact our health. The blue curve in Fig. 5(c) shows the Raman spectrum of an spinach leaf after fluorescence subtraction (See Supplement 1 for more data). We observe molecular fingerprints of carotinoids and nitrate in our sample [annotated C and N in Fig. 5(c)]. Both of these nutrients are associated with numerous benefits from heart to eye health [22,23]. We also observed a peak near 1307 cm^{-1} which is present in many anthocyanins such as peonidin and cyanidin. Besides nutritional value, anthocyanins and carotinoids are stress markers in plants and important chemicals to monitor in farming [24]. Here, the total spectral acquisition time was increased to 52 s to increase the SNR—compared to the measurement of pharmaceutical tablets which are at much higher concentrations. We believe our detection limit for nitrate is below 0.3% (w/w) as the maximum regulated concentration level of nitrate in fresh spinach is 3000 mg/kg [22].

Finally, we measured the limit of detection (LOD) of methanol mixed in an alcoholic drink—a common cause of alcohol poisoning [6]. Figure 6(a) shows spectra of vodka (40% alcohol content by volume) spiked with known concentrations of methanol from 0.5% to 4.0% (acquired in a total of 32 s). The C-O stretching bond of methanol increases the Raman intensity near 1020 cm^{-1} . The Raman intensity at 1020 cm^{-1} can be normalized to the intensity of ethanol peak at 1086 cm^{-1} for estimating the methanol concentration and LOD of our Raman setup. In the experiments where only a few Raman peaks are of interest, we can dwell on those peaks for longer to improve the detection limit. Here, we integrate 1020 cm^{-1} and 1086 cm^{-1} bands each at 5 s (a total spectral acquisition time of 10 s) and achieve an LOD of 0.8% (v/v) [Fig. 6(b)] below the maximum tolerable concentration of 2% [25]. We are achieving about 40× better sensitivity for every mW of excitation power for similar integration time compared to handheld dispersive spectrometers [26] (see Supplement 1 for more comparison data).

Methanol spectra also illustrate that SSRS can achieve both high sensitivity and high spectral resolution, allowing us to measure the frequency shift of methanol's C-O stretching bond when mixed with ethanol [compare top and bottom spectra in Fig. 6(c)]. The 1030 cm^{-1} Raman peak in pure methanol (bottom spectrum) is red-shifted to two new peaks by 12 cm^{-1} and 22 cm^{-1} due to hydrogen bonding with water and ethanol molecules present in the alcoholic drink. This illustrates that SSRS is a useful spectroscopy technique for detailed analysis of individual vibrational states.

5. Conclusion

In summary, we have shown that SSRS is a robust technique that works across different molecular fingerprinting applications. It provides orders of magnitude higher light collection power compared to alternative approaches and enables molecular fingerprinting with low-power, compact lasers and detectors. Further enhancement of results shown in this work is possible with multiplexing lasers and detection channels, as well as using higher throughput meta-material or photonic crystal filters [27]. By requiring only low-power sources that could be implemented on integrated photonic platforms [28], SSRS provides a unique opportunity for miniaturization and low-cost manufacturing of Raman spectrometers.

Funding. Deshpande Center for Technological Innovation, Massachusetts Institute of Technology; National Research Foundation Singapore.

Acknowledgments. This research was supported by the Deshpande Center for Technological Innovation (Massachusetts Institute of Technology, USA), and National Research Foundation (NRF), Prime Minister's Office, Singapore under its Campus for Research Excellence and Technological Enterprise (CREATE) program. The work was conducted under Disruptive and Sustainable Technology for Agricultural Precision (DiSTAP), an interdisciplinary research group (IRG) of the Singapore MIT Alliance for Research and Technology (SMART) Center supported by the National Research Foundation (NRF).

We thank Dodd Gray for help with the free-space optical setup for Raman experiments with the Ti:Sapphire laser. We thank Dodd Gray and Gavin West for their constructive feedback for improving the experiments.

Disclosures. A.H.A. is involved in developing Raman spectroscopy technologies at NuSight Photonics.

Data availability. Data underlying the results presented in this paper are not publicly available at this time but may be obtained from the authors upon reasonable request.

Supplemental document. See [Supplement 1](#) for supporting content.

References

1. C. A. F. de Oliveira Penido, M. T. T. Pacheco, I. K. Lednev, and L. Silveira Jr, "Raman spectroscopy in forensic analysis: identification of cocaine and other illegal drugs of abuse," *J. Raman Spectrosc.* **47**(1), 28–38 (2016).
2. A. Paudel, D. Rajjada, and J. Rantanen, "Raman spectroscopy in pharmaceutical product design," *Adv. Drug Delivery Rev.* **89**, 3–20 (2015).
3. C. H. Huang, G. P. Singh, S. H. Park, N.-H. Chua, R. J. Ram, and B. S. Park, "Early diagnosis and management of nitrogen deficiency in plants utilizing raman spectroscopy," *Front. Plant Sci.* **11**, 663 (2020).
4. M. J. Baker, H. J. Byrne, J. Chalmers, P. Gardner, R. Goodacre, A. Henderson, S. G. Kazarian, F. L. Martin, J. Moger, N. Stone, and J. Sulé-Suso, "Clinical applications of infrared and raman spectroscopy: state of play and future challenges," *Analyst* **143**(8), 1735–1757 (2018).
5. K. A. Esmonde-White, M. Cuellar, C. Uerpman, B. Lenain, and I. R. Lewis, "Raman spectroscopy as a process analytical technology for pharmaceutical manufacturing and bioprocessing," *Anal. Bioanal. Chem.* **409**(3), 637–649 (2017).
6. M. Rostrup, J. K. Edwards, M. Abukalish, M. Ezzabi, D. Some, H. Ritter, T. Menge, A. Abdelrahman, R. Rootwelt, B. Janssens, K. Lind, R. Paasma, and K. E. Hovda, "The methanol poisoning outbreaks in Libya 2013 and Kenya 2014," *PLoS One* **11**(3), e0152676 (2016).
7. W. R. McCluney, *Introduction to radiometry and photometry* (Artech House, 2014).
8. R. Goodacre, D. Graham, and K. Faulds, "Recent developments in quantitative sers: Moving towards absolute quantification," *TrAC, Trends Anal. Chem.* **102**, 359–368 (2018).
9. D. B. Chase, "Fourier transform raman spectroscopy," *J. Am. Chem. Soc.* **108**(24), 7485–7488 (1986).
10. V. Saptari, *Fourier transform spectroscopy instrumentation engineering*, vol. 61 (SPIE Press, 2004).
11. B. G. Saar, C. W. Freudiger, J. Reichman, C. M. Stanley, G. R. Holtom, and X. S. Xie, "Video-rate molecular imaging in vivo with stimulated raman scattering," *Science* **330**(6009), 1368–1370 (2010).
12. S. Bégin, B. Burgoyne, V. Mercier, A. Villeneuve, R. Vallée, and D. Côté, "Coherent anti-stokes raman scattering hyperspectral tissue imaging with a wavelength-swept system," *Biomed. Opt. Express* **2**(5), 1296–1306 (2011).
13. D. D. John, C. B. Burgner, B. Potsaid, M. E. Robertson, B. K. Lee, W. J. Choi, A. E. Cable, J. G. Fujimoto, and V. Jayaraman, "Wideband electrically pumped 1050-nm mems-tunable vcsel for ophthalmic imaging," *J. Lightwave Technol.* **33**(16), 3461–3468 (2015).
14. D. D. John, B. Lee, B. Potsaid, A. C. Kennedy, M. E. Robertson, C. B. Burgner, A. E. Cable, J. G. Fujimoto, and V. Jayaraman, "Single-mode and high-speed 850nm mems-vcsel," in *Advanced Solid State Lasers*, (Optical Society of America, 2016), pp. ATh5A–2.
15. N. R. Gomer, C. M. Gordon, P. Lucey, S. K. Sharma, J. C. Carter, and S. M. Angel, "Raman spectroscopy using a spatial heterodyne spectrometer: proof of concept," *Appl. Spectrosc.* **65**(8), 849–857 (2011).
16. C. Burgner, J. Carter, A. Donaldson, N. Bramham, B. Potsaid, O. Carrasco-Zevallos, S. Chen, E. Moulton, J. G. Fujimoto, P. Heim, V. Jayaraman, and A. Cable, "Reliable widely tunable electrically pumped 1050nm mems-vcsels with amplifier in single butterfly co-package," in *Optical Coherence Tomography and Coherence Domain Optical Methods in Biomedicine XXIV*, vol. 11228 (International Society for Optics and Photonics, 2020), p. 1122809.
17. C. L. Haynes, A. D. McFarland, and R. P. Van Duyne, "Surface-enhanced raman spectroscopy," *Anal. Chem.* **77**, 338 A–346 A (2005).
18. World Health Organization, "A study on the public health and socioeconomic impact of substandard and falsified medical products," World Health Organization (2017).
19. C. Tondepu, R. Toth, C. V. Navin, L. S. Lawson, and J. D. Rodriguez, "Screening of unapproved drugs using portable raman spectroscopy," *Anal. Chim. Acta* **973**, 75–81 (2017).
20. D.-Z. Mao, X.-X. Weng, and Y.-J. Yang, "Rapid screening of sildenafil and tadalafil adulterated in healthcare products by micro-raman spectroscopy," *J. Raman Spectrosc.* **43**(12), 1985–1990 (2012).
21. M. de Veij, A. Deneckere, P. Vandenabeele, D. de Kaste, and L. Moens, "Detection of counterfeit viagra® with raman spectroscopy," *J. Pharm. Biomed. Anal.* **46**(2), 303–309 (2008).
22. P. Santamaria, "Nitrate in vegetables: toxicity, content, intake and ec regulation," *J. Sci. Food Agric.* **86**(1), 10–17 (2006).
23. B. Demmig-Adams and W. W. Adams, "Antioxidants in photosynthesis and human nutrition," *Science* **298**(5601), 2149–2153 (2002).
24. N. Altangerel, G. O. Ariunbold, C. Gorman, M. H. Alkahtani, E. J. Borrego, D. Bohlmeier, P. Hemmer, M. V. Kolomiets, J. S. Yuan, and M. O. Scully, "In vivo diagnostics of early abiotic plant stress response via raman spectroscopy," *Proc. Natl. Acad. Sci.* **114**(13), 3393–3396 (2017).
25. A. Paine and A. Dayan, "Defining a tolerable concentration of methanol in alcoholic drinks," *Hum. Exp. Toxicol.* **20**(11), 563–568 (2001).
26. D. Ellis, H. Muhamadali, Y. Xu, R. Eccles, I. Goodall, and R. Goodacre, "Rapid through-container detection of fake spirits and methanol quantification with handheld raman spectroscopy," *Analyst* **144**(1), 324–330 (2019).

27. X. Buet, E. Daran, D. Belharet, F. Lozes-Dupuy, A. Monmayrant, and O. Gauthier-Lafaye, "High angular tolerance and reflectivity with narrow bandwidth cavity-resonator-integrated guided-mode resonance filter," *Opt. Express* **20**(8), 9322–9327 (2012).
28. A. H. Atabaki, S. Moazeni, F. Pavanello, H. Gevorgyan, J. Notaros, L. Alloatti, M. T. Wade, C. Sun, S. A. Kruger, H. Meng, K. Al Qubaisi, I. Wang, B. Zhang, A. Khilo, C. V. Baiocco, M. A. Popović, V. M. Stojanović, and R. J. Ram, "Integrating photonics with silicon nanoelectronics for the next generation of systems on a chip," *Nature* **556**(7701), 349–354 (2018).